

Enhanced secondary-ion emission under gold-cluster bombardment with energies from keV to MeV per atom

A. Brunelle,* S. Della-Negra, J. Depauw, D. Jacquet, Y. Le Beyec, and M. Pautrat
Institut de Physique Nucléaire, UMR 8608, CNRS-IN2P3, Université Paris-Sud, 91406 Orsay Cedex, France

K. Baudin
Touzart et Matignon, 2 avenue du Pacifique, 91942 Courtaboeuf Cedex, France

H. H. Andersen
Niels Bohr Institute, Ørsted Laboratory, Universitetsparken 5, DK-2100 Copenhagen Ø, Denmark
 (Received 14 March 2000; published 18 January 2001)

Gold-cluster beams of Au_n^+ , $n=1-4$, have been used to measure the secondary-ion emission from organic (biomolecules) and inorganic (CsI) targets over the very large energy range of 4 keV to 10 MeV per atom. The nonlinear enhancement of secondary-ion emission yields with regard to the constituent number in the cluster projectiles is shown to vary with the incident velocity and the type of secondary ions. For complex secondary ions, the yields as a function of the projectile energy per atom present an unexpected maximum around 50–80 keV per atom. The yields increase again above 1 MeV per atom.

DOI: 10.1103/PhysRevA.63.022902

PACS number(s): 79.20.Rf, 36.40.-c, 34.50.Dy

I. INTRODUCTION

The bombardment of solids by different kinds of particles (photons, electrons, and atomic and polyatomic ions) has been studied for many years by different groups and review papers have recently been published on this subject [1]. The total sputtering and emission of atomic ions from metallic surfaces are relatively well understood, but the emission from organic and inorganic surfaces and the emission of complex polyatomic ions such as molecules and clusters are subjects that are still being widely discussed. Several groups are studying these topics, which are of the utmost importance to gaining a better knowledge of the processes governing the emission of clusters and polyatomic species.

Additional information on the interaction between the projectile and the solid target can be obtained through the use of polyatomic ions as projectiles, which give the unique possibility of bombarding simultaneously a very small area with several atoms. Several review papers have been published recently [2,3]. The use of such projectiles leads to a strong increase of the energy density deposited and overlap between the cascades started by individual atoms. Enhanced total sputter yields under cluster impacts were observed already by Andersen and Bay [4] more than 20 years ago. Bismuth and antimony clusters were also used by Thompson and Johar [5]. The authors of Ref. [4] found that the sputtering yield induced by a tellurium dimer (Te_2^+) was higher than twice that induced by the atomic projectile Te^+ at the same velocity of 200 keV per atom. This was called a “non-linear enhancement” of the secondary emission. For impact of larger clusters, it is useful to define the following ratio, as was done in [6]:

$$\mathcal{E}_m^n = \frac{mY_n}{nY_m} \quad \text{with } n > m, \quad (1)$$

Y_n and Y_m being the emission yields induced at identical impact velocities by projectiles having n and m constituents, respectively. If different from 1, the ratio \mathcal{E}_m^n reflects the “nonadditivity” of the emission yields under polyatomic impacts, which means that the emission yields obtained with different clusters of the same type are not directly proportional to their number of constituents. It is called an enhancement factor in [6] if larger than 1. More recently, metal total sputtering yields under gold-cluster bombardment (Au_n , $n=1-5$ [7] and $n=1-13$ [8]), with energies from 20 keV/at to a few MeV/at, have been measured. Strong enhancement factors of the sputtering yields are observed with a maximum reaching a value of 3000 gold atoms ejected per Au_5 impact at 200 keV/at, while only 55 atoms are ejected by a single Au_1 projectile at the same velocity, i.e., the enhancement factor \mathcal{E}_1^5 is larger than 10, while enhancement factors up to 20 will be reported in [8].

Even though the ionization probability is unknown, much can still be learned from a study of the ionized fraction of the emitted species. This secondary-ion emission has previously been studied with impacts of gold-cluster ions Au_n^+ ($n=1-5$) and C_{60}^+ fullerene ions in the keV energy range (from a few keV/at to ~ 20 keV/at for Au_n^+) with different kinds of organic and inorganic target samples [6,9,10], and with Au_n^- ($n=1-4$) impacting metal targets [11–13]. Particularly in [6], a strong increase of the secondary-ion yields corresponding to a large enhancement factor \mathcal{E}_1^2 was observed between the secondary-ion yields induced by gold dimers and monomers, respectively. For larger values of n , the yields were found to scale with n^2 at a given velocity. It is because of these particularly high desorption efficiencies that some authors have started to use clusters and polyatomic ions as projectiles for analytical purposes [14–19]. In the MeV per atom energy range, hydrogen [20] and C_nH_m [21] clusters were the first to be used to induce secondary-ion emission. Enhancement factors larger than 1 were also ob-

*Corresponding author. Email address: brunelle@ipno.in2p3.fr

served at these energies for the secondary-ion emission. One should note that the energy loss of these fast projectiles is governed by electronic excitations instead of collisions with the atoms of the bulk. In recent years, it has become possible with tandem accelerators to have beams of heavy clusters such as C_{10} , C_{60} , and Au_4 with a few MeV of energy [22–24]. The secondary emission of organic molecular ions and clusters under impacts of Au_n^+ ($n=1-3$) projectiles has been studied between ~ 2 and ~ 7 MeV per atom [25], leading to a similar $\sim n^2$ power-law variation. The n^2 variation is in the MeV energy range valid for all n values in contrast to the keV energy range. Further, Tomaschko *et al.* [26] also measured nonadditive enhancements of $(CsI)_pCs^+$ secondary-ion emission under bombardment of C_n^+ ($n=1-12$, 0.714 MeV/at), Ag_n^+ ($n=1-7$, 1.1 MeV/at), and Au_n^+ ($n=1-5$, 2 MeV/at) clusters, i.e., in the high-energy part of the present experiments for Au_n^+ projectiles.

The aim of the present work was to study secondary-ion emission from different kinds of organic and inorganic targets under the impact of gold clusters over the largest possible range of energy per atom, from 4 keV/at to 5 MeV/at.

II. EXPERIMENT

Gold-cluster ion beams Au_n^+ with $n=1-4$ were provided by three different beam facilities, depending on the following energy ranges.

(i) From 4 to ~ 30 keV, a pulsed liquid metal ion source as described in Ref. [6] was used.

(ii) Above ~ 150 keV, the 15-MV IPN-Orsay Tandem accelerator was used to produce the pulsed Au_n^+ gold-cluster ion beams by a method analogous to a normal tandem operating mode. The clusters are characterized through the procedure described in Ref. [24].

(iii) From ~ 30 keV to ~ 3.5 MeV, the 2-MV Aramis tandem accelerator [27], located at the CSNSM Laboratory at Orsay, was used.

The energy ranges from the Tandem and from Aramis overlapped, and the data obtained with these two facilities agreed within 15%, as can be seen in Fig. 2 and Fig. 7. In (ii) and (iii), the beams with the lowest energy per atom were 37.5 keV/at Au_4^- (Tandem) and 33 keV/at Au_3^- negative ions (Aramis). These beams were injected into the accelerator without any stripping gas at the terminal. Under these conditions, the final cluster energy at the exit of the accelerator is equal to the injection energy.

During the experiments, two different systems for the extraction of secondary ions were used: one had a gridless double electrode extractor and the other a 90% transmission grid. Figure 1 shows the experimental setup without grids. Pulsed cluster beams pass through a 2-mm-diam aperture and hit subsequently the target surface in the experimental chamber maintained at a pressure of 10^{-5} Pa by a cryopump. The angle of impact was always 45° . Secondary electrons and negative ions emitted from the target are accelerated with a high voltage (-6 to -18 kV) between the target and the gridless double electrode extractor placed in front of the target. They fly 20 cm before hitting a set of dual chevron microchannel plates (MCP) of 18 mm diam. The output sig-

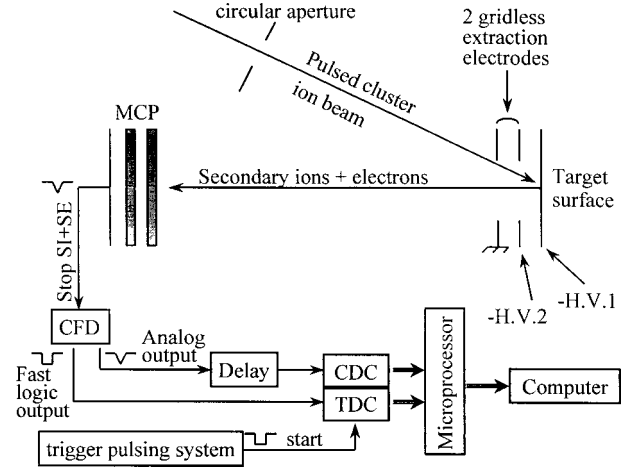


FIG. 1. Schematic view of the experimental setup used for measurements of secondary-ion emission yields under cluster impact.

nal of the detector is split into two signals: one is fed into a constant fraction discriminator (CFD) for time-of-flight measurements with the multistop time-to-digital converter (TDC), which is triggered either by the beam trigger pulsing system or by the arrival of the secondary electrons onto the MCP; the second, which is an analog signal proportional to the number of electrons or ions hitting the MCP, is fed into a charge-to-digital converter (CDC) that is time correlated with the TDC [28]. The measured secondary-ion emission yields Y_{meas} are calculated as the ratio of the number of detected secondary ions over the number of primary ions. By assuming a Poisson distribution for the ion emission, the measured yields were corrected as follows to get the true yields Y_{true} [29]:

$$Y_{\text{true}} = -\frac{1}{\varepsilon} \ln(1 - Y_{\text{meas}}) \quad (2)$$

with ε being the geometrical efficiency of the microchannel plates (approximately 0.6). This ε , which could not be absolutely determined, was arbitrarily chosen to be 1 in this paper. The uncertainty of Eq. (2) becomes too large if Y_{meas} is close to 1. Consequently, for Y_{meas} values larger than 0.5, Eq. (2) was replaced by [30,31]:

$$Y_{\text{true}} = \frac{1}{\varepsilon} n_{\text{meas}} Y_{\text{meas}}, \quad (3)$$

where n_{meas} is the mean number per impact of ions of a given mass obtained from the CDC and Y_{meas} now being equivalent to the probability to detect at least one ion [$Y_{\text{meas}} = 1 - P(0)$, $P(0)$ being the probability of no ion emission].

As already mentioned above, another experimental setup was utilized with the secondary-ion extraction accomplished with a single 90% transmission grid. This setup, not shown here, has been described in detail in a previous paper [32], in which secondary electrons emitted from a CsI target under the impact of the same Au_1 to Au_4 cluster ion beams were studied. Since the 90% transmission grid intercepts the projectile ion beam at an angle of 45° , 13–15% of the ions may

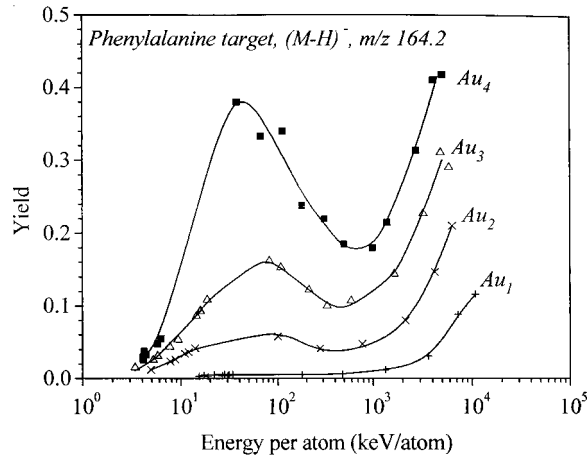


FIG. 2. Secondary-ion emission yield of the negative molecular ion $(M-H)^-$, $m/z=164.2$, from a Phenylalanine target, as a function of energy per atom of the Au_n^+ cluster projectiles, $n=1-4$. The solid lines are to guide the eye.

hit the grid wires, causing desorption of secondary ions from contaminant layers present at the grid surface. The transmission T_θ of a grid at an angle θ with respect to the normal is

$$T_\theta = (1 - e/a)^2 \left(1 - \frac{e/a}{1 - e/a} \tan \theta \right)$$

for wires with a square section,

$$T_\theta = (1 - e/a)^2 \left(\frac{\frac{1}{1 - e/a} \cos \theta - \frac{e/a}{1 - e/a}}{\cos \theta} \right)$$

for wires with a circular section,

e and a being the wire thickness and the grid spacing, respectively. The desorbed ions are accelerated by the electric field between the grid and the target and induce further secondary electron and ion emission from the target. In the present case of cluster impacts, this disturbing effect is reinforced because of the high desorption efficiency of clusters. It is necessary to discriminate the events due to the impacts on grid wires from the “true” events due to the direct impacts of cluster ions on the target surface. All of the results shown in this paper were obtained either after rejection of the events due to grid-induced emission, in agreement with the method described in [32], or with gridless extraction electrodes (present setup, Fig. 1). After correction of the grid effects, the two setups give comparable results, as shown in the subsequent figures.

The quality of the targets with regard to damage, surface contamination, and secondary-ion emission was checked by time-of-flight mass spectrometry with fission fragments from a ^{252}Cf source, which could at any time be inserted behind the targets. When not bombarded by the cluster ion beam, the targets were all maintained in a vacuum airlock having the same pressure and residual gas quality as the experimental chamber.

The targets used were vapor deposited onto aluminized Mylar foils ($1.5\text{-}\mu\text{m}$ thickness) as 200 nm of CsI or Pheny-

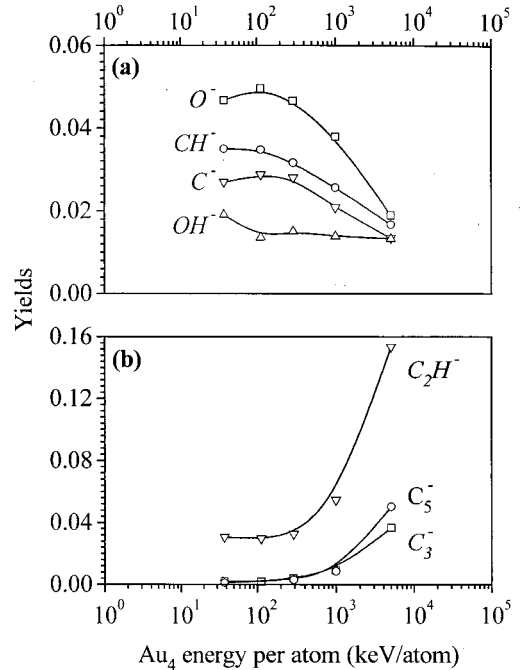


FIG. 3. Secondary-ion emission yield of the following negative light mass fragment ions: (a) C^- , CH^- , O^- , and OH^- , $m/z = 12, 13, 16,$ and 17 , respectively; (b) C_2H^- , C_3^- , and C_5^- , $m/z = 25, 36,$ and 60 , respectively, from a Phenylalanine target, as a function of the energy per atom of Au_4^+ projectiles. The solid lines are only to guide the eye.

alanine [$C_9H_{11}O_2N$, molecular weight (MW) of 165.2 u], or by electrospraying of a lipid ethylene glycol solution (lipid EG, $C_{22}H_{44}O_{11}NP$, MW of 529.6 u). A series of clusters can be emitted from a CsI deposit, which is easy to prepare in thin layers. Phenylalanine is a rather light organic compound also easy to prepare in thin layers with a good reproducibility, and for which we had already published data both in the keV [6] and MeV [25] impact energy ranges. In addition to these two compounds, and having in mind a possible analytical application, the efficiency of the gold clusters was tested on a heavy mass organic compound with a lipid-EG target also used in Ref. [6].

III. RESULTS AND DISCUSSION

A. Secondary-ion emission as a function of the projectile energy per atom

Figures 2–8 show secondary-ion emission yields, as defined above. These figures are a representative selection from many more ion yield results, which have been measured but are not shown. The yields are presented as a function of energy per atom (keV/atom) of the incident gold cluster ions Au_n^+ , $n=1-4$. The use of a scale proportional to v^2 for the abscissa is convenient for a direct comparison of the secondary-ion emission yields induced by cluster projectiles having different sizes but the same velocity. The low-energy points for the deprotonated molecular ion from Phenylalanine, $(M-H)^-$, in Fig. 2 were taken from Ref. [6] (the yields induced by the fission fragments of the ^{252}Cf source were the same in [6] and in the present experiments).

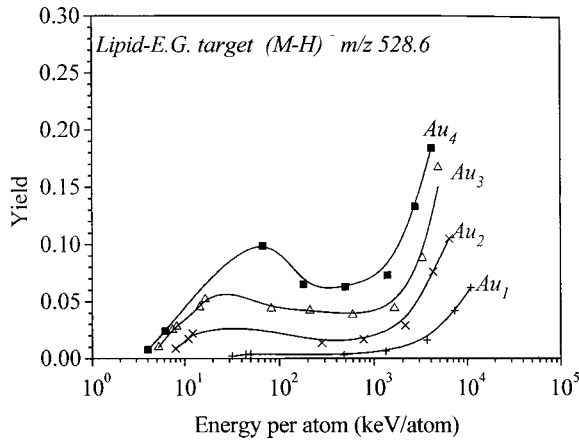


FIG. 4. Secondary-ion emission yield of the negative molecular ion $(M-H)^-$, $m/z=528.6$, from a lipid-EG target, as a function of the energy per atom of the Au_n^+ cluster projectiles, $n=1-4$. The solid lines are to guide the eye.

Although the experimental setup used here is obviously not designed for absolute measurements of secondary-ion initial kinetic-energy distributions, a detailed analysis of the ion peak shapes in the time-of-flight spectra discloses some useful information about the secondary-ion initial axial kinetic energy.

1. Phenylalanine target

In Fig. 2, we show the yield variations of the negative molecular ion $(M-H)^-$. While it is continuously increasing with energy under monatomic gold ion bombardment, a different variation is observed with Au_2 , Au_3 , and Au_4 clusters. A maximum of yield is reached at about 40 keV/at. Above this maximum, the secondary-ion emission yields decrease and reach a minimum around 0.5–1.0 MeV/at, and finally increase again above ~ 1 MeV/at. Below 30 keV/at and above ~ 2 MeV/at, the secondary-ion emission yields were previously known to increase linearly with the energy per

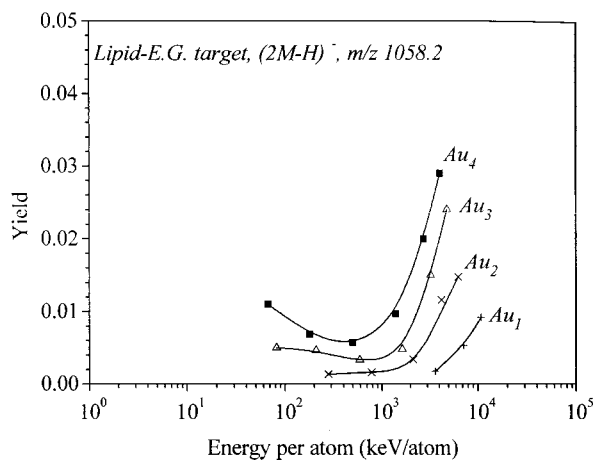


FIG. 5. Secondary-ion emission yield of the negative dimer ion $(2M-H)^-$, $m/z=1058.2$, from a lipid-EG target, as a function of the energy per atom of the Au_n^+ cluster projectiles, $n=1-4$. The solid lines are to guide the eye.

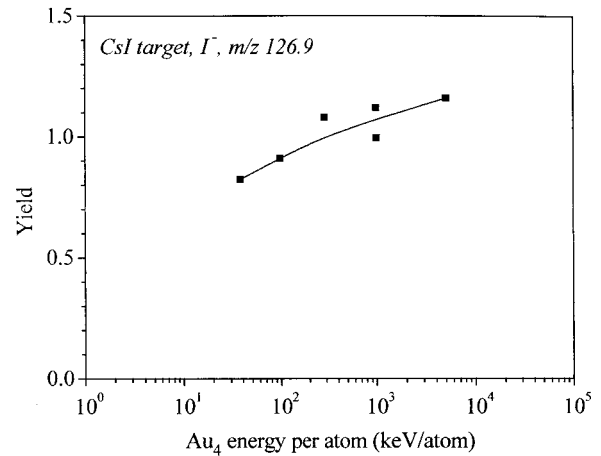


FIG. 6. Secondary-ion emission yield of the negative ion I^- , $m/z=126.9$, from a CsI target as a function of energy per atom of the Au_4^+ projectiles. The solid line is a guide to the eye.

atom of the projectiles (i.e., proportional to the square of the velocity) [6,25], but the humped curve shapes of the yields in the intermediate energy range of $\sim 40-80$ keV/at was rather unexpected.

The secondary-ion emission yields of the light ions C_2H^- , C_3^- , and C_5^- measured under the impacts of Au_4^+ clusters increase with energy over the whole energy range, while the C^- , CH^- , O^- , and OH^- ion yields decrease above 100 keV/at (Fig. 3). The mass peaks of these last four secondary ions exhibit tails towards shorter times, corresponding to maximum energies of 800–1000 eV, while the other ions from this target have only very small tails corresponding to less than 10 eV.

The H^- ions desorbed by Au_3^+ and Au_4^+ have also been studied (not shown). It appears that their yields do not depend on the energy of the projectiles (in the energy domain investigated) and are almost proportional to the number of constituents in the projectile [$Y(H^-)/n$ is constant and independent of velocity], which is in agreement with [6].

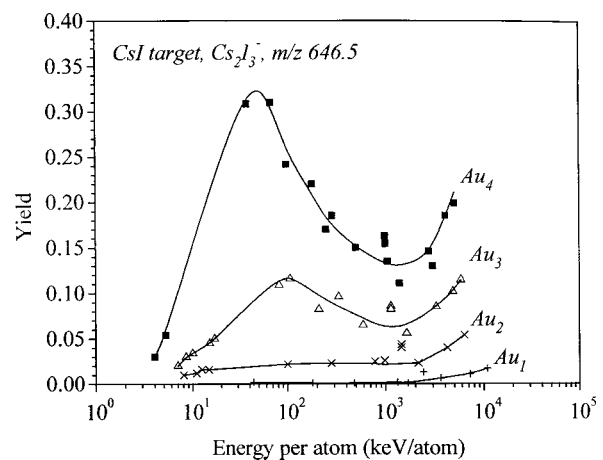


FIG. 7. Secondary-ion emission yield of the negative cluster ion $Cs_2I_3^-$, $m/z=646.5$, from a CsI target, as a function of the energy per atom of the Au_n^+ cluster projectiles, $n=1-4$. The solid lines are to guide the eye.

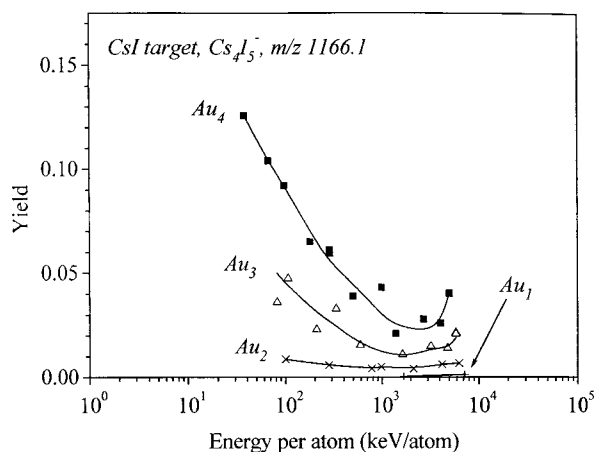


FIG. 8. Secondary-ion emission yield of the negative cluster ion Cs_4I_5^- , $m/z = 1166.1$, from a CsI target, as a function of the energy per atom of the Au_n^+ cluster projectiles, $n = 1-4$. The solid lines are to guide the eye.

2. Lipid-EG target

Figures 4 and 5 show the yields of the negative molecular ion and of the dimer ion, respectively, from the lipid-EG target. Few experimental points were obtained in the keV energy range for the dimer ion (the yields with this target were too small in this energy range). Nevertheless, the yield variations are similar to the molecular ion ($M\text{-H}^-$) from the Phenylalanine target, although the targets had very different molecular masses. The light mass ions (as in Fig. 3) were not investigated for this target.

3. CsI target

Figure 6 shows the yield variation of the I^- secondary ion under the bombardment of Au_4 clusters. This curve slowly increases in the measured energy range. Few experimental points are shown in this figure because a part of the experiment was performed without the CDC [which gives the value of n_{meas} in Eq. (3)] so that high yield values could not be measured. The yields of the Cs_2I_3^- and Cs_4I_5^- ions shown in Figs. 7 and 8 are very similar to the yields of the molecular ion ($M\text{-H}^-$) of Phenylalanine (Fig. 2). Although, in the case of the Cs_4I_5^- ion we have no experimental points at energies lower than 40 keV/at, a comparison between Figs. 7 and 8 (Cs_2I_3^- and Cs_4I_5^- ion yields) tends to show that the slope above the yield maximum is much more pronounced when the size of the secondary ion increases, while the increase above 1 MeV is less evident.

All the light mass ions H^- , C_2H^- , C_3^- , C_5^- , C^- , CH^- , O^- , and OH^- are also desorbed from the CsI target. These ions result from organic surface contaminant layers and their yields (not shown) are very similar to the case of the Phenylalanine target.

Concerning the ion mass peak shapes, the I^- ion peak also has a shorter time-of-flight tail, corresponding to an initial energy larger than 100 eV. When comparing the I^- ion peaks obtained under Au_4^+ impacts at 37.5 keV/at and 5.04 MeV/at, respectively, one observes that the relative importance of

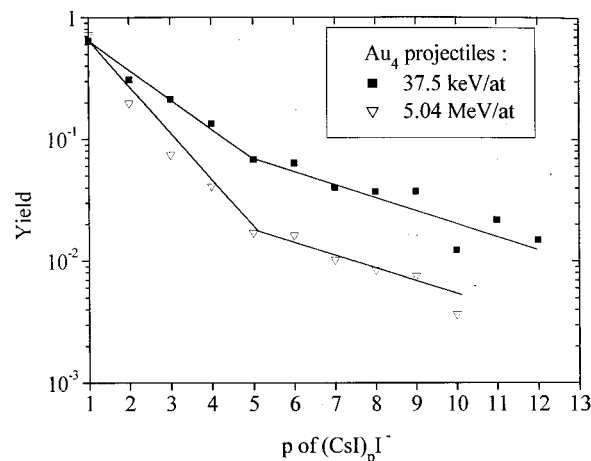


FIG. 9. Secondary-ion emission yields of the $(\text{CsI})_p\text{I}^-$ cluster ions as a function of their size p , and for two different Au_4^+ projectile energies, 37.5 keV/at and 5.04 MeV/at, respectively. The solid lines are to guide the eye.

the tail is smaller at a high impact velocity than at a low energy. It is known that the desorption due to elastic collisions is characterized by higher initial kinetic energies than in the inelastic collision regime [33]. This supports the idea that along the large impact energy scale, different mechanisms exist for the desorption and ionization of the various secondary ions. Also interesting are the longer time-of-flight tails of the $(\text{CsI})_p\text{I}^-$ cluster ions, indicating the CsI clusters to have an energy deficit. In addition, those tails are more important with decreasing impact energy and are more important under polyatomic than under atomic ion impacts. Several assumptions may be evoked to explain such a behavior: a part of the ions may be ionized somewhat in front of the target surface after their desorption as neutrals, leading to a smaller acceleration; they could also be emitted with a short time delay after the impact of the projectile, or they could be slowed by collisions with the other particles emitted (the impact of 200 keV/at Au_4 projectiles onto gold releases more than 1500 gold atoms into the gas phase [7]). Further specific experiments have to be done to obtain more information on the kinetic-energy distributions of the ions desorbed by cluster impacts. Recent experiments of Belykh *et al.* [13] have shown that kinetic energies of large secondary cluster ions desorbed by polyatomic ions are larger than the kinetic energies of large secondary cluster ions desorbed by atomic ions.

B. Yields as a function of secondary-ion size

It has already been said above (compare Figs. 7 and 8) that the larger the size of the secondary ions, the more pronounced is the maximum of the yields around 40 keV/at. A similar trend is seen from Fig. 9, which shows the yields of $(\text{CsI})_p\text{I}^-$ secondary cluster ions as a function of their size p under impact of Au_4 projectiles at 37.5 keV/at (close to the maximum of the yield values) and at 5.04 MeV/at, respectively. These variations of yields with size are called yield distributions in the following. It was unfortunately not pos-

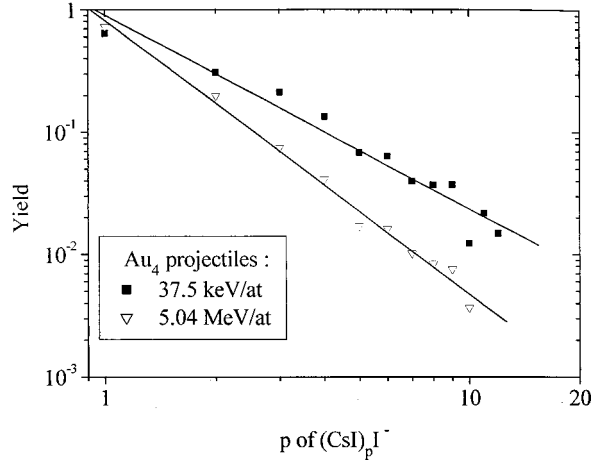


FIG. 10. Same as Fig. 9 but with a log scale as the abscissa. The solid lines are power-law fits: $Y(p) = kp^{-\delta}$ (see text).

sible to show a valid comparison with atomic projectiles, because the counting rates of large secondary clusters ($p \geq 3$) were too low to give yields with a reasonable accuracy. For “small” clusters $p \leq 4$ [but $p = 4$ for a $(\text{CsI})_p \text{I}^-$ cluster means nine atoms, all having approximately the same mass], the relative abundance rapidly decreases with increasing p , and with a slope higher at 5.04 MeV/at of impact energy than at 37.5 keV/at. For “heavy” clusters $p > 4$, both distributions have the same slope independently of the projectile energy and the yields measured at the lowest energy are about four times greater than those measured at the highest energy. The change of slope in Fig. 9 indicates that large secondary cluster ions are probably formed through a mechanism different from that of small ones. With similar observations, Belykh *et al.* in [13] come to the same conclusion, although their results concern Au_1 to Au_3 at 6–18 keV/at ejecting Nb_p and Ta_p clusters from metallic surfaces. It is possible to summarize the behavior of secondary cluster ion yield distributions as follows:

- (i) For “small” size secondary cluster ions [$(\text{CsI})_p \text{I}^-$, $p \leq 4$], the yield distributions are independent of the size of the projectile and decrease more rapidly for high projectile impact energies than for low energies,
- (ii) For “large” secondary cluster ions ($p > 4$), the yield distributions are independent of the energy of the cluster projectile.

Although Fig. 9 clearly shows that the decrease of $(\text{CsI})_p \text{I}^-$ cluster yields as function of their size p cannot follow a unique law over the investigated values of p , it is also interesting to redraw Fig. 9 with log-log scales on both axes for comparison with what is usually done in the literature. In Fig. 10, the same yields roughly follow a $p^{-\delta}$ power law with δ equal to 1.6 ± 0.12 and 2.3 ± 0.08 at 37.5 keV/at and 5.04 MeV/at, respectively. A small increase of δ with energy per atom (not shown) is found. Similar slopes have been observed for Ta_p^+ and Nb_p^+ ion emission under keV energy gold-cluster bombardment by Belykh *et al.* [34]. Under atomic ion impacts, a faster decrease with the size of secondaries is observed by Ens *et al.* for cesium iodide cluster ions desorbed by keV energy Cs^+ ions ($\delta \approx 3$) [35] and

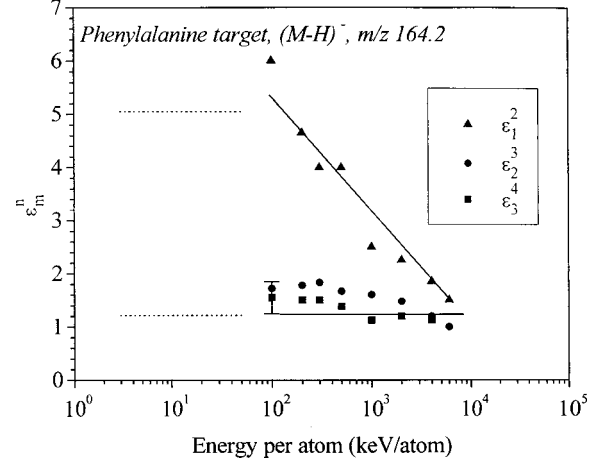


FIG. 11. Enhancement factors [as defined in Eq. (1)] for the negative molecular ion $(M-H)^-$, $m/z = 164.2$, from a Phenylalanine target, as a function of the energy per atom of Au_n^+ cluster projectiles, $n = 1-4$. The solid lines are to guide the eye and the dashed lines have been added from [6].

by Wahl and Wucher for sputtering of Ag_p^0 and Ag_p^+ by 5-keV Ar^+ ions ($\delta \leq 4$) [36]. Theoretical treatments based on a thermodynamic equilibrium [37] and on a shock wave model [38], respectively, both lead to values of δ close to 2 for the distribution of secondary cluster ions. Another model by Wucher based on a combination of molecular dynamics and Monte Carlo simulations concerns the yield distribution of neutral metal clusters. He also finds a $p^{-\delta}$ power law, but with δ values between 4 and 7 depending strongly on the bombarding conditions [39]. More recently, the same author found the δ exponent to be experimentally related to the total sputtering yield: the higher the total sputtering yield, the smaller the value of δ [40]. Of course, one should be very prudent with these comparisons of different power laws found in the literature. First of all, Figs. 9 and 10 have shown that log-log scales may hide important variations in the measured yield distributions, and second, different experimental conditions and especially different detection efficiencies as a function of secondary ion mass could lead to wrong conclusions when comparing δ values. However, values of δ as small as 2 cannot be due to a smaller detection efficiency for large rather than small clusters in the present experiments.

C. Secondary-ion yields as a function of the projectile number of constituents

Enhancement factors \mathcal{E}_m^n , as defined above by the relation (1), which are useful to highlight the nonadditive behavior of the secondary-ion emission with regard to the size of the projectiles, are shown in Figs. 11, 12, and 13 for the negative molecular ion $(M-H)^-$ from the Phenylalanine target and for the negative cluster ions Cs_2I_3^- and Cs_4I_5^- from the CsI target, respectively. It was previously observed in the velocity range studied in [6] (a few keV to a few tens of keV) that all the \mathcal{E}_m^n were larger than 1, independent of the projectile velocity (dashed lines shown for comparison in Fig. 11), and were increasing linearly with the n/m ratio. Around 100

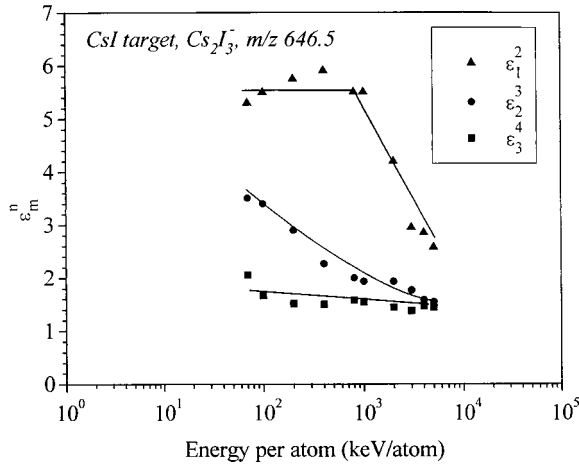


FIG. 12. Enhancement factors [as defined in Eq. (1)] for the negative Cs_2I_3^- cluster ion, $m/z=646.5$, from a CsI target, as a function of the energy per atom of the Au_n^+ cluster projectiles, $n=1-4$. The solid lines are to guide the eye.

keV/at and for the same secondary ion, the values of \mathcal{E}_m^n in Fig. 11 are comparable to those obtained in [6] for Phenylalanine: a strong enhancement of the secondary-ion emission is observed between the atomic and the dimer projectiles ($\mathcal{E}_1^2 > 5$) and the other \mathcal{E}_m^n (with $n-m=1$) values are close to ~ 1.5 .

In the present experiments, the enhancement factors \mathcal{E}_m^n behave as follows.

\mathcal{E}_1^2 : For Phenylalanine at 100 keV/at it is larger than 5 and decreases above this energy to reach a value smaller than 2. For Cs_2I_3^- , a plateau is observed between 100 keV/at and 1 MeV/at at a value larger than 5, followed by a decrease, but the enhancement factor is still larger than 2 at the highest energy per atom. These values mean that the yields roughly scale with n^2 at high energy per atom and with n^3 (or n^γ with $\gamma \geq 3$) at low energy per atom. A similar decrease is

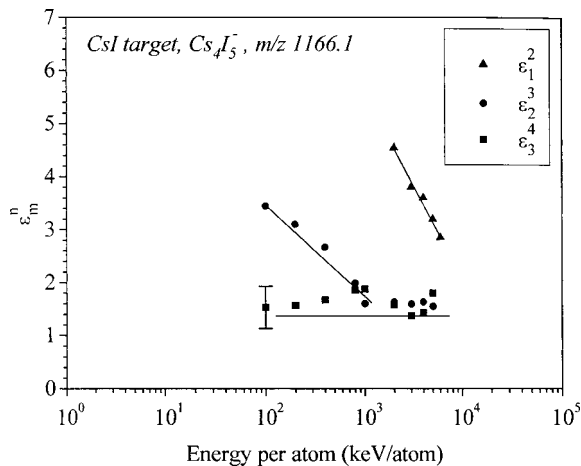


FIG. 13. Enhancement factors [as defined in Eq. (1)] for the negative Cs_4I_5^- cluster ion, $m/z=1166.1$, from a CsI target, as a function of the energy per atom of the Au_n^+ cluster projectiles, $n=1-4$. The solid lines are to guide the eye.

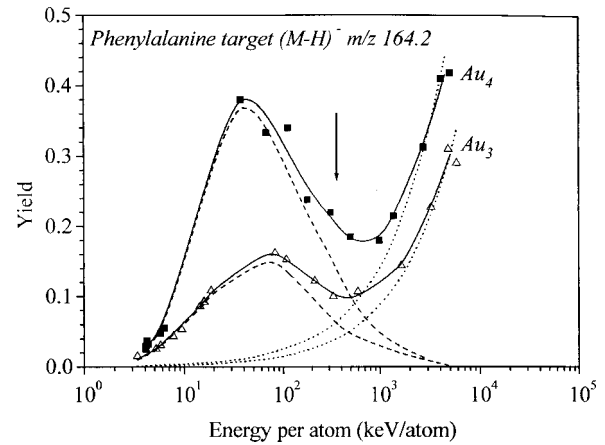


FIG. 14. Experimental yields of the negative molecular ion $(\text{M-H})^-$, $m/z=164.2$, from a Phenylalanine target, as a function of the energy per atom of Au_3^+ and Au_4^+ cluster projectiles, compared to functions proportional to $(dE/dx)_{\text{ele}}^2$ of gold into Lexan (a plastic compound similar to Phenylalanine) calculated with the SRIM code [44] (dotted lines). Dashed lines are the experimental yields to which the electronic stopping power contributions have been subtracted. The vertical arrow indicates the energy for which the calculated nuclear stopping power is maximum in this compound (~ 380 keV).

observed for Cs_4I_5^- , although it is not possible to tell if a plateau exists or not.

\mathcal{E}_2^3 : It lies between 1 and 2 for Phenylalanine, close to $3/2$. This value of $3/2$ for the enhancement factor corresponds to yields scaling with n^2 . For the CsI clusters, it is continuously decreasing from ~ 3.5 at 100 keV/at to $\sim 3/2$ at 1 MeV/at and above.

\mathcal{E}_3^4 : For the Phenylalanine and the CsI clusters, it is close to $4/3$.

Finally, for $n \geq 2$ for Phenylalanine and for $n \geq 3$ for CsI, all the \mathcal{E}_m^n (with $n-m=1$) are close to n/m , which is equivalent to yields scaling with n^2 , and an increase of the yields faster than n^2 is observed for energies per atom smaller than 500 keV/at.

D. Comparisons between secondary-ion yields and nuclear or electronic stopping powers

In this section, the stopping power $dE/dx(n)$ of a cluster having n identical atomic constituents is assumed to be n times the stopping power dE/dx of one atom at the same velocity. This assumption is based on the recent projected range measurements of gold implanted as Au_1 , Au_2 , and Au_3 , which were found experimentally to be independent of cluster size at a given velocity [41]. The same conclusion was also obtained for MeV energy C_n ($n=1-8$) clusters losing their energy through electronic excitations [42].

The yields of C^- , CH^- , O^- , and OH^- secondary ions [Fig. 3(a)] vary with energy as the square of the nuclear stopping power in organic layers (and CsI layers) and decrease with increasing energy, while the yields of the carbon and hydrocarbon clusters [Fig. 3(b)] increase as the square of the electronic stopping power. Both nuclear and electronic

stopping powers probably contribute to the I^- ion yield (Fig. 6). The behavior of these ion yields with regard to stopping powers is similar to the analysis made by Hunt *et al.* with Xe^+ projectiles [43], who concluded that the nuclear stopping power played a dominant role in the desorption process of atomic and light mass ions, in a form similar to classical sputtering. For other ions such as C_2H^- , the variation follows $(dE/dx)_{ele}^2$.

The above comparisons between stopping powers and atomic or light mass ion yield are not straightforward with complex secondary ions such as the deprotonated Phenylalanine negative molecular ion and the CsI cluster ions, although for these ions the emission yields induced by an atomic projectile follow $(dE/dx)_{ele}^\alpha$ (α between 2 and 3) over the whole energy range. It is very different for the yields measured with cluster projectiles. Only the increase of the ion yields above ~ 1 MeV/at can be attributed to phenomena governed by the electronic stopping power as shown in Figs. 14 and 15. The dotted lines in these two figures are proportional to calculated [44] values of $(ndE/dx)_{ele}^\alpha$, with $\alpha=2$ for Phenylalanine and $\alpha=1.5$ for CsI, respectively. Although the code used only accounts for single atom impacts,¹ the comparison is justified with the above assumption (at the beginning of Sec. III D). Hunt *et al.* observed that organic secondary-ion yields under atomic ion bombardment evolved as $(dE/dx)_{ele}^2$ [43], like the yields under atomic gold bombardment in the present experiments. Tomaschko *et al.* found in [26] that Cs^+ and Cs_2I^+ ion yields were scaling with $[n(dE/dx)_{ele} - S]^\alpha$ ($\alpha=2.5$ and 2.9 for Cs^+ and Cs_2I^+ , respectively, and S being a threshold value) under C_n^+ bombardment at 0.714 MeV/at, but the electronic stopping power dominates for carbon clusters at this energy. It is possible to conclude that in the high-energy part (above ~ 1 MeV/at) of the yield curves, the secondary-ion yields still follow a certain power of the electronic energy loss. It is possible to subtract from the yield curves the contributions (dotted lines) of the electronic stopping power. The resulting dashed lines in Figs. 14 and 15 show consequently the part of the ion yields that are not due to the electronic stopping power. The same procedure can be applied for all the complex secondary ions (not shown). The consequence is that they have the same humped curves with, in particular, the same decreasing slopes for $Cs_2I_3^-$ and $Cs_4I_5^-$ ions. For gold-cluster projectiles penetrating into Phenylalanine or CsI, the maxima of the yields are reached for a much smaller energy than the energy per atom of the maxima of nuclear stopping powers. This is illustrated in Figs. 14 and 15 by the vertical arrows placed at energies for which the nuclear stopping powers are maxima for gold into Lexan (~ 380 keV) and gold into CsI (~ 550 keV), respectively. If the nuclear stopping power is responsible for the rapid increase of the yields below the maxima, another

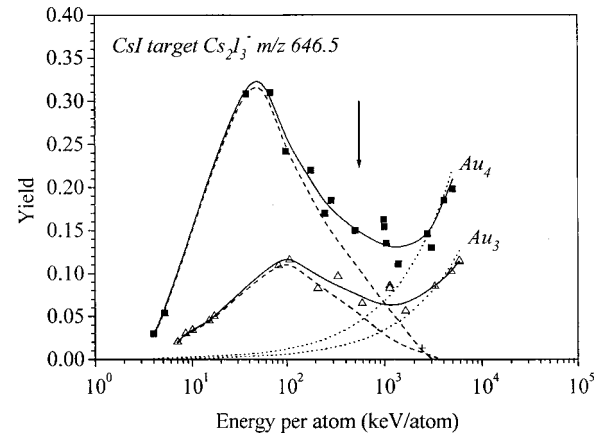


FIG. 15. Same as Fig. 14 but for the $Cs_2I_3^-$ ion from the CsI target. The vertical arrow indicates the energy for which the calculated nuclear stopping power is maximum in this compound (~ 550 keV).

unknown effect occurs above the maxima that strongly reduces the observed secondary-ion yields. A variation of the ionization probability could be evoked, but could hardly explain the difference in yield variations between atomic and polyatomic secondary ions. With increasing deposited energy, the number of sputtered particles increases drastically, increasing consequently the number of collisions between escaping ions with the result that polyatomic secondary ions would dissociate before or during their acceleration in the mass spectrometer. In the present experiments, the characteristic time necessary to accelerate the secondary ions is of the order of 100 ns, which means that we can only observe unfragmented ions surviving this time. Metastable ions may decay in the drift tube and the resulting fragment ions that keep the same velocity as their precursors are not time-separated from stable ions. We do not discuss here the possibility of collisions between polyatomic secondary ions and other target atoms on their way to the surface as this appears very unlikely.

It may be tempting to correlate the range of the projectile in the target at the velocity corresponding to the maxima of secondary-ion emission with an optimal depth of desorption (that would depend on the material sample) [45–49]. Several models of desorption (see, for example, [50] and [51]) with atomic projectiles in the electronic stopping energy domain refer to critical pressure (and critical energy density) with a radius of ejected volume, cylindrical or hemispherical. Large craters were observed in organic samples when using fast clusters as projectiles [52,53]. In the nuclear energy-loss regime, large-size craters were also observed at the surface of gold foils bombarded by gold clusters [8], which clearly prove that secondary emission phenomena are not restricted to the surface.

IV. CONCLUSION

The maximum rate of ion emission is observed at much lower velocity than the velocity of the maximum of the linear energy loss by nuclear collisions. In experiments with gold metal targets bombarded by gold clusters in the same

¹The SRIM 2000 code was used. For Phenylalanine, the variations with incident energy of the electronic and nuclear energy losses have been calculated for a single gold atom penetrating Lexan, a plastic compound having similar density and stoichiometry to Phenylalanine.

energy range, it was observed that the highest total sputtering yields also occur at lower velocity than the velocity of the maximum nuclear stopping power [7]. Recent results with Au_n projectiles, $n = 1 - 13$ [8] and also $n \approx 80$, confirm the previous results obtained with Au_1 to Au_5 . The general experimental trend is thus an emission rate probability (ions and neutrals) at a relative low value of the nuclear stopping power. In these giant emission phenomena, many parameters are involved and further experimental data need to be collected before having a clear picture of the processes. In the present state, a modeling of these experimental results seems to be very difficult on such a large scale of energy studied (this has never been done before). However, this work, and

also recent work with Au_n ($n = 1 - 13$), shows that the domain of velocity of 30 to ~ 100 keV/at with heavy cluster projectiles is very attractive for further study: the release of matter from solids and surface material modifications are important and there are potential applications with such beams.

ACKNOWLEDGMENTS

The Aramis (CSNSM) and IPN-Orsay Tandem accelerator groups are gratefully acknowledged for their technical support during the experiments. One author (H.H.A.) thanks the Danish National Science Research Council (SNF) for a grant that enabled his participation in the above experiments.

-
- [1] Fundamental Processes in Sputtering of Atoms and Molecules, edited by Peter Sigmund [Mat. Fys. Medd. K. Dan. Vidensk. Selsk. **43**, (1993)].
- [2] H. H. Andersen, in [1], p. 127.
- [3] Y. Le Beyec, Int. J. Mass Spectrom. Ion Processes **174**, 101 (1998).
- [4] H. H. Andersen and H. L. Bay, J. Appl. Phys. **45**, 953 (1974); **46**, 2416 (1975).
- [5] D. A. Thompson and S. S. Johar, Appl. Phys. Lett. **34**, 342 (1979).
- [6] M. Benguerba, A. Brunelle, S. Della-Negra, J. Depauw, H. Joret, Y. Le Beyec, M. G. Blain, E. A. Schweikert, G. Ben Assayag, and P. Sudraud, Nucl. Instrum. Methods Phys. Res. B **62**, 8 (1991).
- [7] H. H. Andersen, A. Brunelle, S. Della-Negra, J. Depauw, D. Jacquet, Y. Le Beyec, J. Chaumont, and H. Bernas, Phys. Rev. Lett. **80**, 5433 (1998).
- [8] S. Bouneau, A. Brunelle, S. Della-Negra, J. Depauw, D. Jacquet, Y. Le Beyec, M. Pautrat, M. Fallavier, J. C. Poizat, H. H. Andersen (unpublished).
- [9] K. Boussofiane-Baudin, A. Brunelle, G. Bolbach, S. Della-Negra, P. Håkansson, and Y. Le Beyec, Nucl. Instrum. Methods Phys. Res. B **88**, 160 (1994).
- [10] M. J. Van Stipdonk, R. D. Harris, and E. A. Schweikert, Rapid Commun. Mass Spectrom. **10**, 1987 (1996).
- [11] S. F. Belykh, I. S. Bitensky, D. Mullajanov, and U. Kh. Rasulev, Nucl. Instrum. Methods Phys. Res. B **129**, 451 (1997).
- [12] S. F. Belykh, U. Kh. Rasulev, A. V. Samartsev, and I. V. Veryovkin, Nucl. Instrum. Methods Phys. Res. B **136**, 773 (1998).
- [13] S. F. Belykh, B. Habets, U. Kh. Rasulev, A. V. Samartsev, L. V. Stroev, and I. V. Veryovkin, Nucl. Instrum. Methods Phys. Res. B **164-165**, 809 (2000).
- [14] A. D. Appelhans and J. E. Delmore, Anal. Chem. **61**, 1087 (1989).
- [15] W. Szymczak and K. Wittmaack, Nucl. Instrum. Methods Phys. Res. B **88**, 149 (1994).
- [16] J. F. Mahoney, D. S. Cornett, and T. D. Lee, Rapid Commun. Mass Spectrom. **8**, 403 (1994).
- [17] G. Gillen and S. Roberson, Rapid Commun. Mass Spectrom. **12**, 1303 (1998).
- [18] K. Iltgen, C. Bendel, A. Benninghoven, and E. Niehuis, J. Vac. Sci. Technol. A **15**, 460 (1997).
- [19] F. Kötter and A. Benninghoven, Appl. Surf. Sci. **133**, 47 (1998).
- [20] J. P. Thomas, P. E. Filpus-Luickx, M. Fallavier, and E. A. Schweikert, Phys. Rev. Lett. **55**, 103 (1985).
- [21] M. Salephour, D. L. Fistel, and J. E. Hunt, Phys. Rev. B **38**, 12 320 (1988).
- [22] K. Boussofiane-Baudin, A. Brunelle, P. Chaurand, J. Depauw, S. Della-Negra, P. Håkansson, and Y. Le Beyec, Int. J. Mass Spectrom. Ion Processes **130**, 73 (1994).
- [23] S. Della-Negra, A. Brunelle, Y. Le Beyec, J. M. Curaudeau, J. P. Mouffron, B. Waast, P. Håkansson, B. U. R. Sundqvist, and E. S. Parilis, Nucl. Instrum. Methods Phys. Res. B **74**, 453 (1993).
- [24] Ch. Schoppmann, P. Wohlfart, D. Brandl, M. Sauer, Ch. Tomaschko, H. Voit, K. Boussofiane, A. Brunelle, P. Chaurand, J. Depauw, S. Della-Negra, P. Håkansson, and Y. Le Beyec, Nucl. Instrum. Methods Phys. Res. B **82**, 156 (1993).
- [25] K. Boussofiane-Baudin, A. Brunelle, P. Chaurand, S. Della-Negra, J. Depauw, P. Håkansson, and Y. Le Beyec, Nucl. Instrum. Methods Phys. Res. B **88**, 61 (1994).
- [26] Ch. Tomaschko, K. H. Hermann, J. Käshammer, R. Kügler, Ch. Schoppmann, and H. Voit, Nucl. Instrum. Methods Phys. Res. B **132**, 371 (1997).
- [27] H. Bernas, J. Chaumont, E. Cottureau, R. Meunier, A. Traverse, C. Clerc, O. Kaitasov, F. Lalu, D. Le Du, G. Moroy, and M. Salomé, Nucl. Instrum. Methods Phys. Res. B **62**, 416 (1992).
- [28] J. C. Cuzon, Annual Report, IPN 83-13 (unpublished); S. Della-Negra and Y. Le Beyec, in *Proceedings of SIMS VI Conference, Versailles, 1987*, edited by A. Benninghoven (Wiley, New York, 1988); G. B. Baptista, A. Brunelle, P. Chaurand, S. Della-Negra, J. Depauw, Y. Le Beyec, Rapid Commun. Mass Spectrom. **5**, 632 (1991).
- [29] P. Håkansson and B. U. R. Sundqvist, Radiat. Eff. **61**, 179 (1982).
- [30] A. Brunelle, P. Chaurand, S. Della-Negra, Y. Le Beyec, and G. B. Baptista, Int. J. Mass Spectrom. Ion Processes **126**, 65 (1993).
- [31] A. Brunelle, P. Chaurand, S. Della-Negra, Y. Le Beyec, and E. Parilis, Rapid Commun. Mass Spectrom. **11**, 353 (1997).
- [32] K. Baudin, A. Brunelle, S. Della-Negra, J. Depauw, Y. Le

- Beyec, and E. S. Parilis, Nucl. Instrum. Methods Phys. Res. B **117**, 47 (1996).
- [33] K. Wien, Radiat. Eff. Defects Solids **109**, 137 (1989).
- [34] S. F. Belykh, I. S. Bitensky, D. Mullajanov, and U. Kh. Rasulev, Nucl. Instrum. Methods Phys. Res. B **129**, 451 (1997).
- [35] W. Ens, R. Beavis, and K. G. Standing, Phys. Rev. Lett. **50**, 27 (1983).
- [36] M. Wahl and A. Wucher, Nucl. Instrum. Methods Phys. Res. B **94**, 36 (1994).
- [37] H. M. Urbassek, Nucl. Instrum. Methods Phys. Res. B **31**, 541 (1988).
- [38] I. S. Bitensky and E. S. Parilis, Nucl. Instrum. Methods Phys. Res. B **21**, 26 (1987).
- [39] A. Wucher, Nucl. Instrum. Methods Phys. Res. B **83**, 79 (1993).
- [40] A. Wucher and M. Wahl, Nucl. Instrum. Methods Phys. Res. B **115**, 581 (1996).
- [41] H. H. Andersen, A. Johansen, M. Olsen, and V. S. Tuboltsev (unpublished).
- [42] K. Baudin, A. Brunelle, M. Chabot, S. Della-Negra, D. Gardes, P. Håkansson, Y. Le Beyec, A. Billebaud, M. Fallavier, J. Remillieux, J. P. Thomas, and J. C. Poizat, Nucl. Instrum. Methods Phys. Res. B **94**, 341 (1994).
- [43] J. E. Hunt, M. Salehpour, D. L. Fishel, and J. C. Tou, J. Phys., Colloq. C2 **50**, 27 (1989).
- [44] J. F. Ziegler, J. P. Biersack, and H. Littmark, *The Stopping and Ranges of Ions in Solids* (Pergamon, New York, 1985).
- [45] G. Säve, P. Håkansson, B. U. R. Sundqvist, and U. Jönsson, Nucl. Instrum. Methods Phys. Res. B **26**, 571 (1987).
- [46] K. Wien, O. Becker, W. Guthier, S. Della-Negra, Y. Le Beyec, B. Monart, K. G. Standing, G. Maynard, and C. Deutsch, Int. J. Mass Spectrom. Ion Phys. **78**, 273 (1987).
- [47] G. Bolbach, S. Della-Negra, C. Deprun, Y. Le Beyec, and K. G. Standing, Rapid Commun. Mass Spectrom. **1**, 22 (1987).
- [48] S. Della-Negra, J. Depauw, H. Joret, Y. Le Beyec, I. S. Bitensky, G. Bolbach, R. Galera, and K. Wien, Nucl. Instrum. Methods Phys. Res. B **52**, 121 (1990).
- [49] R. Schmidt, Ch. Schoppmann, D. Brandl, A. Ostrowsky, H. Voit, D. Johannsmann, and W. Knoll, Phys. Rev. B **44**, 560 (1991).
- [50] C. T. Reimann, Mat. Fys. Medd. K. Dan. Vidensk. Selsk. **43**, 351 (1993).
- [51] I. S. Bitensky, A. M. Goldenberg, and E. S. Parilis, J. Phys. Colloq. C2 **50**, 213 (1989).
- [52] C. Tomaschko, M. Schurr, R. Berger, G. Saemann-Ischenko, H. Voit, A. Brunelle, S. Della-Negra, and Y. Le Beyec, Rapid Commun. Mass Spectrom. **9**, 924 (1995).
- [53] D. D. N. Barlo Daya, A. Hallen, J. Eriksson, J. Kopniczky, R. Papaléo, C. T. Reimann, P. Håkansson, B. U. R. Sundqvist, A. Brunelle, S. Della-Negra, and Y. Le Beyec, Nucl. Instrum. Methods Phys. Res. B **106**, 37 (1995).